CORA Cork Open Research Archive
Cartlann Taighde Oscailte Chorcaí

Title	Advancing atomic nanolithography: cold atomic Cs beam exposure of alkanethiol self-assembled monolayers
Authors	O'Dwyer, Colm;Gay, G.;Viaris de Lesegno, B.;Weiner, J.;Mutzel, M.;Haubrich, D.;Meschede, D.;Ludolph, K.;Georgiev, G.;Oesterschulze, E.
Publication date	2005-01
Original Citation	O'Dwyer, C., Gay, G., Lesegno, B., Viaris de,Weiner, J., Mutzel, M., Haubrich, D., Meschede, D., udolph, K., Georgiev, G. and Oesterschulze, E. (2005) 'Advancing atomic nanolithography: cold atomic Cs beam exposure of alkanethiol self-Assembled monolayers', Journal of Physics: Conference Series, 19, pp. 109-117. http://stacks.iop.org/1742-6596/19/i=1/a=019
Type of publication	Article (peer-reviewed)
Link to publisher's version	10.1088/1742-6596/19/1/019
Rights	© 2005 IOP Publishing Ltd.
Download date	2026-09-17 10:11:51
Item downloaded from	https://hdl.handle.net/10468/2825

UCC
University College Cork, Ireland
Coláiste na hOllscoile Corcaigh

Advancing atomic nanolithography: cold atomic Cs beam exposure of alkanethiol self assembled monolayers

C O'Dwyer [1,2], G Gay [1], B Viaris de Lesengo [1,3], J Weiner [1], M Mützel [4], D Haubrich [4], D Meschede [4], K Ludolph [5], G Georgiev [5] and E Oesterschulze [5]

[1] Institut de Recherche sur les Systèmes Atomiques et Moléculaires Complexes, Laboratoire Collisions, Agrégats et Réactivité, UMR CNRS 5589, Université Paul Sabatier, 118 route de Narbonne, 31062 Toulouse Cedex 4, France

[2] Photonic Nanostructures Group, Tyndall National Institute, Lee Maltings, Prospect Row, Cork, Ireland

[3] Laboratoire Aimé Cotton, Campus d'Orsay, 91405 Orsay, France

[4] Institut für Angewandte Physik, Universität Bonn, Wegelerstr. 8, 53115 Bonn, Germany

[5] Institute of Microstructure Technology and Analytics, University of Kassel, 34132 Kassel, Germany

E-mail: codwyer@tyndall.ie

Abstract. We report the results of a study into the quality of functionalized surfaces for nanolithographic imaging. Self-assembled monolayer (SAM) coverage, subsequent post-etch pattern definition and minimum feature size all depend on the quality of the Au substrate used in atomic nanolithographic experiments. We find sputtered Au substrates yield much smoother surfaces and a higher density of $\{111\}$ oriented grains than evaporated Au surfaces. A detailed study of the self-assembly mechanism using molecular resolution AFM and STM has shown that the monolayer is composed of domains with sizes typically of 5-25 nm, and multiple molecular domains can exist within one Au grain. Exposure of the SAM to an optically-cooled atomic Cs beam traversing a two-dimensional array of submicron material

masks ans also standing wave optical masks allowed determination of the minimum average Cs dose (2 Cs atoms per SAM molecule) and the realization of < 50 nm structures. The SAM monolayer contains many non-uniformities such as pin-holes, domain boundaries and monoatomic depressions which are present in the Au surface prior to SAM adsorption. These imperfections limit the use of alkanethiols as a resist in atomic nanolithography experiments. These studies have allowed us to realize an *Atom Pencil* suitable for deposition of precision quantities of material at the micro- and nanoscale to an active surface.

1. Introduction

Self-assembled monolayers (SAMs) of thiol-functionalized molecules on single-crystal Au surfaces have been studied by numerous groups since their discovery [1, 2]. Such organosulfur monolayers now have numerous technological applications, the most recent of which involves their use as positive resists in atomic nano-fabrication [3, 4]. This application has motivated a considerable research effort focusing on their structure, assembly mechanism and experimental parameter dependencies. In the light of recent technological advances in atom beam nanolithography, a detailed understanding of the quality of coverage of the Au surface by the alkanethiol monolayer is necessary to determine its limitations as a uniform resist for feature definition on the order of 5-25 nm. As will be shown however, defect formation in the SAM itself can also occur on single crystal atomically flat surfaces, thus limiting defect-free feature sizes to approximately 20 nm.

In this paper, we present results of a detailed study of the structure of 1-nonanethiol self-assembled monolayers on a polycrystalline Au surface together with the results of a study into the dependency of SAM coverage, subsequent post-etch pattern definition and minimum feature size on the quality of the Au substrate used in both material mask and optical mask atomic nanolithographic experiments. In particular, this paper addresses the essential properties required for optimization and reliable performance of submicron SAM patterning on Au substrates by wet-etching techniques. We alo present results of the application of this technique in the realization of a versatile tool that writes arbitrary structures by atomic

deposition in a serial lithographic process.

2. Experimental

A self-assembled monolayer composed of 1-nonanethiol, $CH_3(CH_3)_8SH$ (95%, Aldrich), was grown on sputterd Au substrates from solution phase in reagent grade ethanol with a nominal thickness $\sim$1 nm. The crystallinity characterization was carried out by grazing incidence X-ray diffraction (GIXRD) [5] with a step width of 0.01°, using a Philips PW-1710 diffractometer with a Cu anode (radiation K_α of λ = 1.54186 Å). X-ray rocking curves were acquired of the substrate and Cr layer in order to obtain the physical rocking curve of the Au overlayer by substraction and deconvolution of all spectra. AFM and STM characterization was performed with a PicoSPM (Molecular Imaging, Inc.). The STM tips were mechanically cut from 250 μm Pt/Ir (80:20) wire, electrochemically etched/polished and tested on highly ordered pyrolytic graphite (HOPG). The STM images were acquired at a bias voltage of +1.50 V in constant height mode. All atomic force microscopy (AFM) and scanning tunneling microscopy (STM) examinations were performed in ambient laboratory conditions (pressure and temperature). AFM and STM characterization was performed with a PicoSPM (Molecular Imaging, Inc.) and a Nano-R AFM (Pacific Nanotechnologies, Inc.). Atomic resolution AFM imaging was performed in both contact and AC tapping modes supplemented by lateral force and phase modulation imaging respectively. Througout the text, the sputtered surface is termed Au:1 and the evaporated surface is termed Au:2.

Further detailed descriptions of process parameters, etching techniques, laser cooling, material and optical masks and substrate preparation can be found elsehwere [6, 7]. Schematically, the exposure and development of the SAM is shown in Fig. 1. A concise description of the *Atom Pencil* can be found in Ref. [8].

3. Results and discussion

In Fig. 2(a) the structure of 1-nonanethiol is outlined schematically. The molecule consists of the sulfur headgroup that bonds with the Au substrate, an alkyl chain and a methyl head group. Fig. 2(b) shows

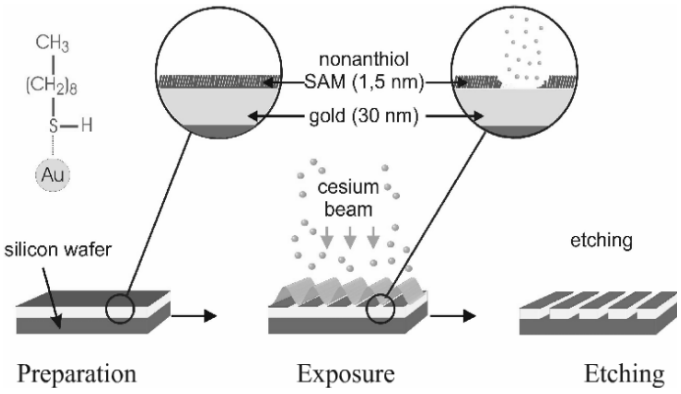

Figure 1. Schematic representation of the exposure and wet-etch development of the SAM covered Au substrate by the cold atomic Cs beam.

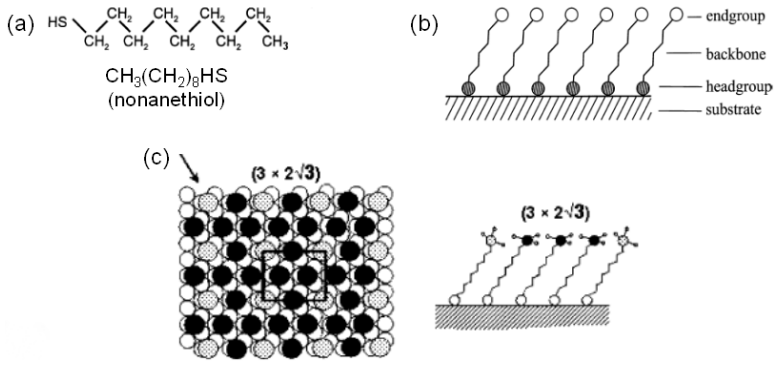

Figure 2. (a) Schematic of the structure of 1-nonanethiol. (b) Representation of alkanethiol adsorption to substrate (c) $(3 \times 2\sqrt{3})$ packing arrangement of 1-nonanethiol on Au$\{111\}$.

how the molecules assemble on the Au surface. The molecules are tilted 30° from the surface normal to the Au in the same direction. The principal packing arrangement when 1-nonanethiol binds to Au$\{111\}$ is shown in Fig. 2(c). The packing arrangement is described as the $(3a \times 2\sqrt{3}a)$ lattice; the unit mesh is highlighted. Here, a is the Au-Au interatomic spacing of the Au$\{111\}$ lattice, equivalent to 0.29 nm. A cross-sectional view is shown alongside the schematic representing the view in the direction of the arrow.

The GIXRD spectrum of the Au overlayer crystal structure is shown in Fig. 3. The data corresponds

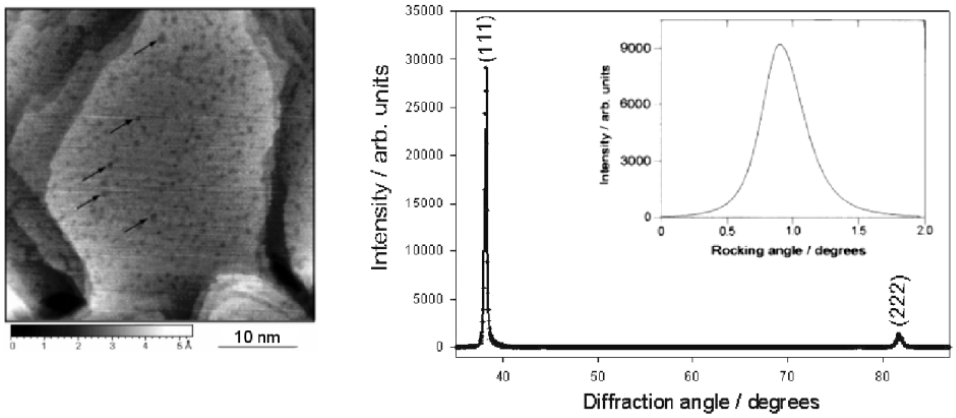

Figure 3. AFM image of the Au{111} surface showing the monatomic terraces. The corresponding GIXRD spectrum and rocking curves are also shown.

to the AFM image of the terraced surface shown alongside the spectrum. Two peaks were observed in the spectrum at 38.15° and 88.3°, which correspond to the {111} and {222} planes of the face-centered cubic structure of bulk Au, respectively. The inter-planar spacing of the sputtered Au layer, determined from the diffraction angle of the {111} plane in Fig. 3, is measured to be 0.238 nm, in good agreement with that of the inter-planar spacing of bulk Au{111} (0.24 nm). The {111} reflection exhibits the highest relative intensity indicating that it is the preferred crystal orientation of the majority of the Au grains within the film. The physical X-ray rocking curve of the Au{111} reflection is shown in the inset to Fig. 3.

Such rocking curves were acquired to determine the minimum grain size of the Au grains parallel to the film, *i.e.* the {111} oriented grains. Utilizing kinematic diffraction theory [9, 10], it is known that

$$FWHM = \frac{\lambda}{2.25 d^{\parallel}_{grain}} \sin\theta \tag{1}$$

where FWHM is the full width at half maximum, $d^{\parallel}_{grain}$ is the minimum grain size parallel to the film and θ is the diffraction angle of the emerging X-rays. This approach determines the minimum grain size to be 137 $\pm$ 13 nm and the alignment of the Au grains to be {111} oriented and parallel to the surface.

Figure 4 shows an STM image of the alkanethiol SAM on the sputtered Au surface. Such large

scale STM surface survey images show the highly variable coverage of the Au by the SAM on Au monatomic terraces. The surface is observed to consist of a mosaic-like network of domains ranging in size from approximately 5-25 nm, with some defect-free domains observed to extend to more than 50 nm. It can also been observed that monolayer domains, highlighted in the image, are present over the full surface area of each terrace. A higher magnification STM image of the monolayer on Au:1 is shown in Fig. 4(b). It can be observed that each domain consists of an ordered arrangement of alkanethiol molecules. Indeed, the packing arrangement is identical and coherent within a single domain, *i.e.* all atoms are arranged such that the unit cell axes of the packing arrangement remain unchanged within the domain itself. Each of the domains are separated by domain boundaries typical of molecular scale dimensions. Such boundaries are identified in Fig. 4(b) as dark fissures between domains. Most boundaries are observed to have three orientations originating from the hexagonal Au$\{111\}$ three-fold surface symmetry, due to the remarkable degree of epitaxy that alkanethiol SAMs have with Au$\{111\}$ surfaces. Even with exceptionally ordered sputtered Au surfaces composed of predominantly $\{111\}$ terminated Au planes, the relative orientation of Au$\{111\}$ grains also adds to the density of nonuniform features. Such boundaries limit the resolution of patterning achievable when SAMs are employed as positive resists in atomic nanolithography experiments.

Non-contact tapping mode AFM was employed to characterize the topography of both the Au:1 and Au:2 surfaces. Figures 5(a) and 5(b) show the surface topography of the Au:1 and Au:2 surfaces respectively. It can be observed that the Au:2 surface is much rougher than that of the Au:1 surface and contains a well pronounced grain structure. The *rms* roughness of the Au:1 and Au:2 surfaces was determined from the AFM data in Figs. 5(a) and 5(b) and is measured to be 1.8 $\pm$ 0.4 nm and 6.7 $\pm$ 1.2 nm respectively. Such smooth Au:1 surfaces are formed by sputtering at low power, which was necessary to produce a smooth surface over a granular 4 nm thick Cr adhesion layer. This smoothness is highlighted more clearly in the magnified image of the surface in Fig. 5(c). In Fig. 5(d), which is a magnified AFM image of the highly granular Au:2 surface shown in Fig. 5(b), the undulating grain

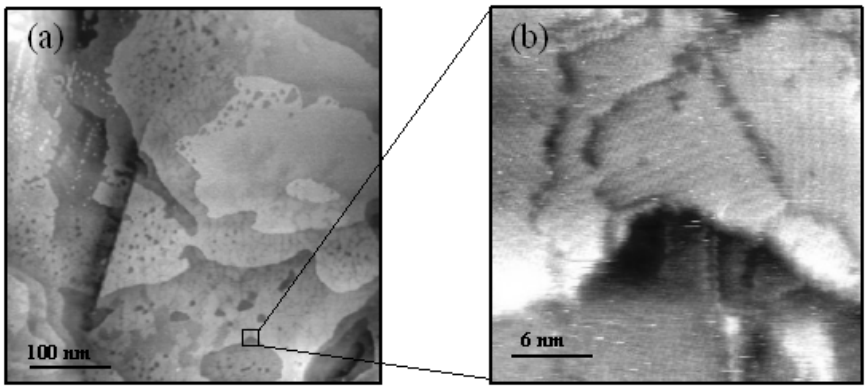

Figure 4. (a) 425 nm $\times$ 425 nm STM image of the SAM on Au$\{111\}$ terraces. (b) 25 nm $\times$ 25 nm STM image of the area highlighted in (a) showing molecular scale domain boundaries and ordered alkanethiol molecule arrangement on Au$\{111\}$ terraces.

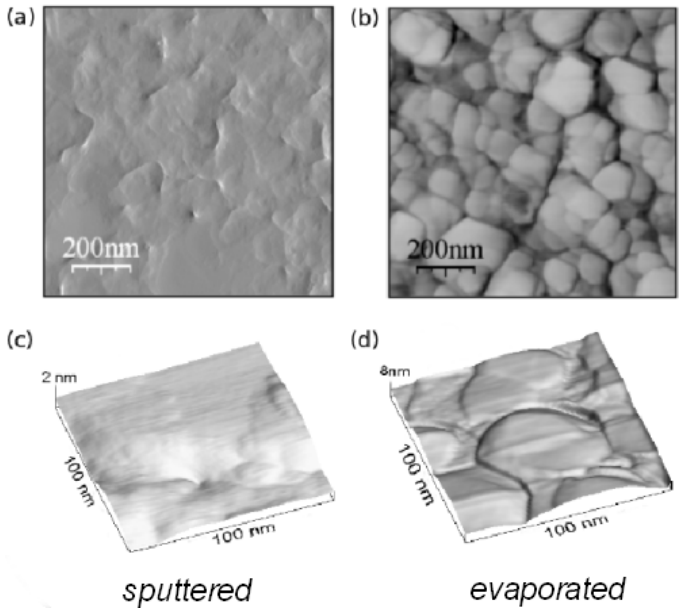

Figure 5. 1 μm $\times$ 1 μm AFM image of (a) the Au:1 surface and (b) the Au:2 surface. (c) 100 nm $\times$ 100 nm higher magnification images of the smooth Au:1 surface and (d) the rougher Au:2 surface where multiple grains can be seen.

structure is clearly observed.

Alkanethiol adsorption is dependent on the crystal orientation of the Au grains but the SAM monolayer uniformity is dependent on the density of grains with the same crystal orientation. Again GIXRD was used to characterize the crystal orientation of the grains in both the Au:1 and Au:2 surfaces and to quantify the relative density of each crystal orientation in both surfaces. The GIXRD spectra of the Au:1 and Au:2 surfaces are shown in Fig. 6(a). For the Au:1 layer, two peaks were observed in the spectrum at 38.15° and 88.3°, which correspond to the $\{111\}$ and $\{222\}$ planes of the face-centered cubic structure of bulk Au, respectively. For the Au:2 layer, however, a number of peaks were observed at 38.15°, 44.35°, 64.6°, 77.9° and 83.8°, corresponding to the $\{111\}$, $\{200\}$, $\{220\}$, $\{311\}$ and $\{222\}$ planes. In both cases, the $\{111\}$ peak shows the highest relative intensity indicating that a greater density of these grains exist in both types of surfaces. However, for the Au:1 surface only two crystal orientations are observed and the difference in relative intensity between these two peaks indicates that the surface is almost entirely composed of $\{111\}$ oriented Au grains. In contrast Au:2 contains a number of crystal orientations; even though the energetically favorable $\{111\}$ grain density is highest. As can be seen from the bottom panel of Fig. 6(a), this density is just a fraction of that for the Au:1 surface. In Fig. 6(b), the normalized $\{111\}$ reflections for both the Au:1 and Au:2 surfaces are overlayed. Individual fitting of the diffraction peaks was carried out by fitting the sample-dependent variables (angle position, intensity and line broadening) to the experimental diffraction profile using a Marquardt nonlinear least-squares algorithm [11]. The Au:1 exhibits a higher relative intensity than the Au:2 surface by a factor of $\sim$1.5. Furthermore, the $\{111\}$ Bragg reflection from the Au:1 surface has a narrower line width indicating the degree of crystallinity in the Au:1 is greater than that of the Au:2 surface. From Fig. 6(a), the quantitative percentage of $\{111\}$ terminated surface on Au:1 and Au:2 can be determined by fitting the rocking curves with a pseudo-Voigt function [12] and a value of 0.94 is determined for this crystal orientation. The fraction of the surface terminated with the $\{111\}$ face for the Au:2 is determined to be 0.49, almost half that for the Au:1 surface.

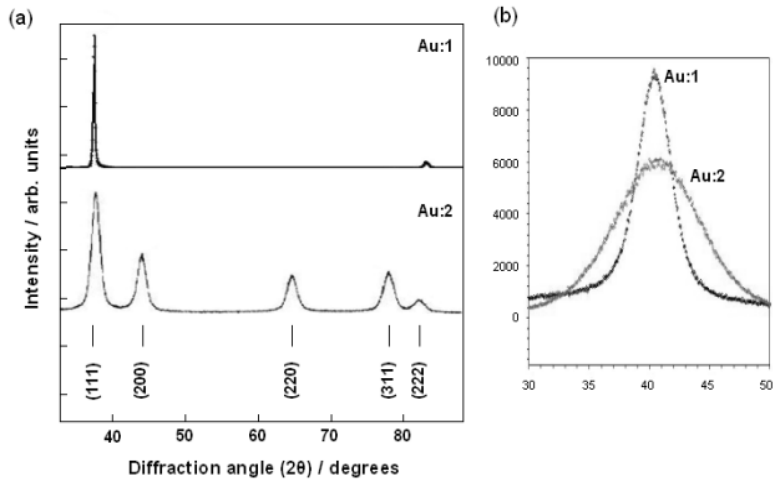

Figure 6. (a) GIXRD spectra of the Au:1 and Au:2 layers. On a logarithmic scale, no discernable peaks from 200, 220 or 311 reflections of the Au lattice could be observed for the Au:1 surface. (b) High resolution normalized GIXRD spectra of the Au:1 and Au:2 layers for the $\{111\}$ peak.

High resolution AFM imaging of the Au:1 surface was also conducted to characterize the surface morphology and growth mechanism of the very smooth grains observed. This imaging technique was not possible, however, for the highly undulating rough Au:2 surface. Figure 7 shows a 200 $\times$ 200 nm AFM image of the Au:1 surface in height-mapped grayscale. A line scan through the 'terraced' area of the surface, indicated on the image, is shown alongside Fig. 7(b). It is observed that the height difference between each of the Au terrace layers is approximately 0.25 nm, almost equivalent to the Au monatomic step height (0.2355 nm), indicating that Au monolayers (defined in the images by the terraces within the grain) are atomically flat and thus single crystal. Highlighted in the image are examples of individual monatomic depressions of the Au surface. Such depressions are noted to be present over the whole surface prior to SAM adsorption and we have recently shown that these pits can increase the defect density of any organic monolayer adsorbed on the surface [6]. Thus, AFM, STM and GIXRD studies of the sputtered Au:1 and evaporated Au:2 surfaces, shows that sputtered Au surfaces exhibit a much lower degree of roughness, and sputtered Au surfaces contain a higher density of $\{111\}$ oriented Au grains, a distinct advantage for the adsorption of alkanethiols [6, 13]. The physical properties for sputtered and

Table 1. Characteristics of the sputtered Au:1 and evaporated Au:2 substrates

	Grain size (nm)	Fraction $\{111\}$ (%)	Roughness (nm)	SAM coverage (%)
Au:1	150	0.94	1.8 ± 0.4	59
Au:2	45	0.49	6.7 ± 1.2	21

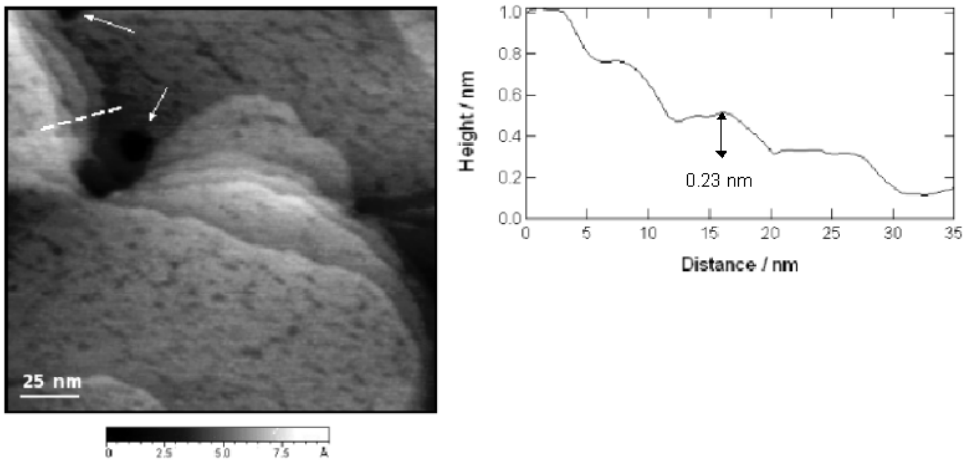

Figure 7. (a) 200 nm $\times$ 200 nm AFM image of the Au:1 surface shown in height-mapped grayscale. Examples of monatomic depressions in the Au surface are highlighted by arrows. (b) Height variation of successive monatomic Au step edges. This data represents the indicator line in the upper left of (a).

evaporated Au surfaces are summarized in Table 1.

The 150 nm size of $\{111\}$ grains on Au:1 surfaces is $\sim$3 times greater than the SAM film thickness, and suggests single-crystal epitaxial growth. Some monatomic depressions exist on the surface of each grain prior to treatment in the alkanethiol solution, but we have recently demonstrated that the alkanethiol covers the surface and depressions alike [6, 13]. Thus sputtered Au films produce good quality substrates for alkanethiol-based resist adsorption for atomic nanolithography applications.

As mentioned above, sputtered substrates give smoother surfaces than evaporated Au surfaces and

show a much lower density of grains. More importantly, however, the Au:1 surface also contains a much greater proportionate density of $\{111\}$ oriented Au grains. The fraction of the surface displaying the crystal faces corresponding to these reflections is important because at least one of them, the $\{100\}$ face, is associated with an incommensurate arrangement of the monolayer lattice and correspondingly weaker SAM-Au bonding. There have been no reports of SAM adsorption on Au$\{200\}$, Au$\{311\}$ or on Au$\{222\}$. Figures 8(a) and 8(b) show non-contact AFM images of the SAM on Au:1 and Au:2 surfaces respectively. Both topographical and phase imaging were acquired simultaneously. Phase imaging allows the determination of the variation in composition of a particular surface. In this case, the alkanethiol monolayer is shown in black and the Au surface is white/bright gray. By numerical integration of monotone phase images, the percentage total coverage of the SAM was found to be 59% and 21% for Au:1 and Au:2 surfaces respectively. Note that the percentage coverage of the Au:1 surface by the SAM is 35% less than its percentage coverage by $\{111\}$ terminated Au faces. The phase imaging information implies therefore that alkanethiol adsorption to other crystal orientations occurs.

Having characterized the influence of the Au surface on the coverage uniformity by the alkanethiol monolayer, we now turn to the exposure of this monolayer by a cold atomic Cs beam. The schematic of the *Atom Pencil* is shown in Fig. 9(a). In the present experiments our key element for writing sub-micron structures is a miniaturized aperture integrated into a hollow pyramidal tip. Figure 9(b) shows a typical structure. Pyramidal tip fabrication is based on two etch processes, a chemical etch to form the pyramid and a plasma etch to form the aperture. Details are described in Refs. [14, 15]. The height of the aperture above the SAM surface $\sim$16 μm. Figure 9(c) shows an AFM image and line profile of the etched SAM. The diameter of the written holes after the standard etch procedure was measured to be 280 nm. The line profile of Fig. 9(c) exhibits very steep flanks. The absolute depth of the hole is about 50 nm and the fractional depth gradient on the side wall is measured to be 0.8/20 nm. This device can be used to deliver precision quantities of material at the micro- and nanoscales to an active surface at much lower energy than ion-implantation techniques and might find application in precision doping of technologically useful

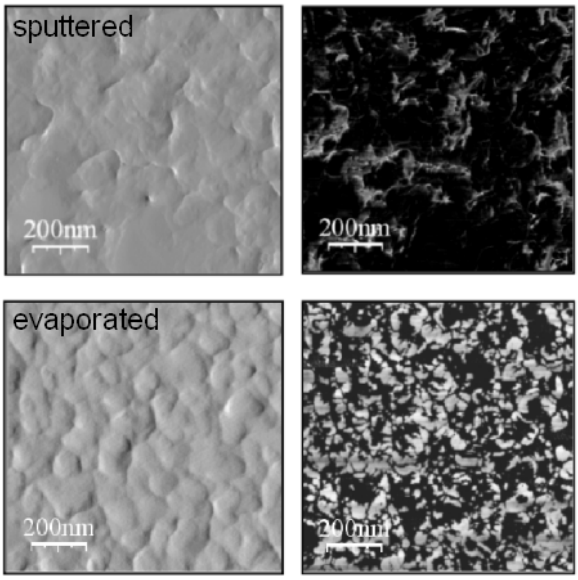

Figure 8. (a) AFM image of the SAM covered Au:1 surface (left panel), and its corresponding phase image (right panel). (b) AFM image (left panel) and corresponding phase image (right panel) for the Au:2 surface covered with the SAM.

materials.

4. Conclusions

We have presented a detailed study of alkanethiol monolayer properties as a function of Au substrates for atomic nanolithography process optimization. We have found the coverage dependency, post-etch pattern definition and submicron features size to be influenced primarily by the quality and morphology of the Au substrate. Sputtered Au substrates yield smoother surface with a higher density of $\{111\}$ oriented grains than evaporated Au surfaces. Phase imaging with AFM shows that that the quality and percentage coverage of uniform alkanethiol monolayer self-assembly is much greater for sputtered Au substrates. Exposure of the monolayer resist with a collimated atomic Cs beam allowed the determina tion of the minimum Cs dose required to alter the Au-S bonding thus exposing the resist. Employing lateral force microscopy, the minimum Cs dose was measured to be 2 Cs atoms per alkanethiol molecule or 2 monolayers of Cs deposited on the SAM surface. Utilizing these results, submicron features as small

Figure 9. (a) The *Atom Pencil* consists of a transversely collimated atomic beam (I) which after a concentration stage (II) is deposited through a pin-hole onto a substrate (III). (b) Pyramidal tips used in the SAM exposure and (c) the resulting etched feature and its corresponding linescan profile.

as $\sim$280 nm were etched into the Au layers using pyramidal aperture masks.

Acknowledgments

This work was supported in part by the European Community's Human Potential Programme under contract HPRN-CT-2002-00304.

References

[1] Schreiber F 2000 *Prog. Surf. Sci.* **65** 151

[2] Ulman A 1996 *Chem. Rev.* **96** 1533

[3] Meschede D and Metcalf H 2003 *J. Phys. D.: Appl. Phys.* **36** R17 and references therein

[4] Camposeo A, Cervelli F, Piombini A, Tantussi F, Fuso F, Allegrini M and Arimondo E 2003 *Mat. Sci. Eng. C* **23** 217

[5] Cullit B D 1978 *Elements of X-ray Diffraction* (Reading: Addison-Wessely)

[6] O'Dwyer C, Gay G, Viaris de Lesegno B and Weiner J 2004 *Langmuir* **20** 8172

[7] O'Dwyer C, Gay G, Viaris de Lesegno B, Weiner J, Ludolph K, Albert D and Oesterschulze E 2005 *J. Appl. Phys.* **97** 114309

[8] Mützel M, Müller M, Haubrich D, Rasbach U, Meschede D, O'Dwyer C, Gay G, Viaris de Lesegno B, Weiner J, Ludolph K, Georgiev G and Oesterschulze E 2005 *Appl. Phys. B* **80**

[9] Berger H 1976 *Krist. Tech.* **11** 1171

[10] Raub E and Muller K 1967 *Fundamentals of Metal Deposition* (Amsterdam: Elsevier) pp 36-38

[11] Nogués J, Costa L and Rao K V 1992 *Physica A* **182** 532

[12] Young R A and Willes D B 1982 *J. Appl. Cryst.* **15** 430

[13] Poirier G E and Tarlov M J 1994 *Langmuir* **10** 285

[14] Vollkopf A, Rudow O and Oesterschulze E 2001 *J. Electrochem. Soc.* **148** G587

[15] Georgiev G, Müller-Wiegand M, Georgieva A, Ludolph K and Oesterschulze E 2003 *J. Vac. Sci. Technol. B* **21** 1361